

This document is confidential and is proprietary to the American Chemical Society and its authors. Do not copy or disclose without written permission. If you have received this item in error, notify the sender and delete all copies.

**Tuning Bandgap of p-type Cu<sub>2</sub>Zn(Sn, Ge)(S, Se)<sub>4</sub> Semiconductor Thin Films via Aqueous Polymer-Assisted Deposition**

Journal:	<i>ACS Applied Materials &amp; Interfaces</i>
Manuscript ID	am-2016-13683b.R1
Manuscript Type:	Article
Date Submitted by the Author:	06-Dec-2016
Complete List of Authors:	Yi, Qinghua; Soochow University, Wu, Jiang; University College London, Electronic and Electrical Engineering Zhao, Jie; Soochow University, Wang, Hao; Soochow University, Hu, Jiapeng; Soochow University Dai, Xiao; Soochow University, Zou, Guifu; Soochow University,

SCHOLARONE™  
Manuscripts

1  
2  
3  
4  
5  
6  
7 Tuning Bandgap of p-type  $\text{Cu}_2\text{Zn}(\text{Sn}, \text{Ge})(\text{S}, \text{Se})_4$   
8  
9  
10  
11 Semiconductor Thin Films via Aqueous Polymer-  
12  
13  
14  
15 Assisted Deposition  
16  
17  
18  
19  
20

21 *Qinghua Yi,<sup>†</sup> Jiang Wu,<sup>§</sup> Jie Zhao,<sup>†</sup> Hao Wang,<sup>†</sup> Jiapeng Hu,<sup>†</sup> Xiao Dai,<sup>†</sup> Guifu Zou<sup>†,\*</sup>*  
22  
23

24  
25 <sup>†</sup> College of Physics, Optoelectronics and Energy & Collaborative Innovation Center of Suzhou  
26  
27

28 Nano Science and Technology, Soochow University, Suzhou 215006, China  
29  
30

31 <sup>§</sup> Department of Electronic and Electrical Engineering, University College London, London  
32  
33

34 WC1E 7JE, UK  
35  
36  
37  
38  
39  
40  
41  
42  
43  
44  
45  
46  
47  
48  
49  
50  
51  
52  
53  
54  
55  
56  
57  
58  
59  
60

**ABSTRACT:** Bandgap engineering of kesterite  $\text{Cu}_2\text{Zn}(\text{Sn}, \text{Ge})(\text{S}, \text{Se})_4$  with well-controlled stoichiometric composition plays a critical role in sustainable inorganic photovoltaics. Herein, a cost-effective and reproducible aqueous solution-based polymer-assisted deposition approach is developed to grow p-type  $\text{Cu}_2\text{Zn}(\text{Sn}, \text{Ge})(\text{S}, \text{Se})_4$  thin films with tunable bandgap. The bandgap of  $\text{Cu}_2\text{Zn}(\text{Sn}, \text{Ge})(\text{S}, \text{Se})_4$  thin films can be tuned within the range 1.05 eV - 1.95 eV using the aqueous polymer-assisted deposition by accurately controlling the elemental compositions. One of the as-grown  $\text{Cu}_2\text{Zn}(\text{Sn}, \text{Ge})(\text{S}, \text{Se})_4$  thin films exhibits a hall coefficient of  $+137 \text{ cm}^3/\text{C}$ . The resistivity, concentration and carrier mobility of the  $\text{Cu}_2\text{Zn}(\text{Sn}, \text{Ge})(\text{S}, \text{Se})_4$  thin film are  $3.17 \text{ ohm}\cdot\text{cm}$ ,  $4.5 \times 10^{16} \text{ cm}^{-3}$ , and  $43 \text{ cm}^2/\text{V}\cdot\text{S}$  at room temperature, respectively. Moreover, the  $\text{Cu}_2\text{Zn}(\text{Sn}, \text{Ge})(\text{S}, \text{Se})_4$  thin film when used as an active layer in a solar cell leads to a power conversion efficiency of 3.55 %. The facile growth of  $\text{Cu}_2\text{Zn}(\text{Sn}, \text{Ge})(\text{S}, \text{Se})_4$  thin films in an aqueous system, instead of organic solvents, provides great promise as an environmental-friendly platform to fabricate a variety of single/multi metal chalcogenides for the thin film industry and solution-processed photovoltaic devices.

**KEYWORDS:** CZTGeSSe, solution processing, bandgap tunable, polymer-assisted deposition, solar cells

## INTRODUCTION

$\text{Cu}_2\text{Zn}(\text{Sn}, \text{Ge})(\text{S}, \text{Se})_4$  (CZTGSSe) is one of the most promising p-type semiconductors in the optoelectronics field due to its low toxicity, cost-efficiency, abundance, high light absorption coefficient and direct bandgap. It has been widely applied to different fields including photocatalysis,<sup>1,2</sup> photovoltaics,<sup>3-6</sup> and biomedicines.<sup>7</sup> More importantly, the CZTGSSe has a tunable bandgap depending on the compositions of Sn, Ge, S, and Se elements.<sup>8,9</sup> It is well known that chemical solution synthesis approaches are effective in precisely controlling the

1  
2  
3 composition of the multicomponent material.<sup>10</sup> Many recent efforts have been devoted to  
4 growing CZTGSSe thin films by chemical solution processes. For example, Mitzi et al. have  
5 fabricated  $\text{Cu}_2\text{Zn}(\text{Sn}, \text{Ge})\text{S}_4$  (CZTGS) thin films by a pure-hydrazine solution approach.<sup>9</sup> The  
6 Moon group used a nanocrystal ink approach to grow CZTGS thin films.<sup>11</sup> These solution-  
7 processed films show great promise as effective light absorber layers in photovoltaic devices.  
8 However, harmful/toxic solvents,<sup>12</sup> complex synthesis, and tedious post-purification<sup>13, 14</sup> limit the  
9 use of these methods to grow CZTGSSe thin films in a viable manner for industry applications.  
10 Therefore, it is highly demanded to develop an alternative environmental-friendly solution route  
11 for synthesis of bandgap tunable CZTGSSe thin films.  
12  
13  
14  
15  
16  
17  
18  
19  
20  
21  
22  
23  
24

25 Water has been well recognized as an ideal and green solvent. However, easily-hydrolyzed  
26 metal ions (e.g. Sn, Ge, etc.) are difficult to form a stable solution in water.<sup>15, 16</sup> Moreover, it is  
27 hard to control the metal ion concentration of the aqueous precursor solution, which often results  
28 in non-stoichiometric growth of the compound thin film. Here, we present a stable metal-ion  
29 aqueous system, comprising a homogeneous metal-polymer complex solution, to grow  
30 single/multiple metal sulfide/selenide thin films. A water-soluble polymer is used to stabilize the  
31 metal ions in precursor solution and facilitate the film coating. Specifically, the metal ions  
32 (nitrates salt, chloride salt) coordinate with lone-pair electrons of the nitrogen atoms in the  
33 polymer preventing hydrolysis of metal ions and hence forming stable metal-polymer  
34 complexes.<sup>17,18</sup> Meanwhile, the non-coordinated anions or cations are easily removed by  
35 filtration processes to prepare a homogeneous precursor solution. By carefully adjusting the  
36 concentration of the Cu, Zn, Sn, and Ge precursors, the final aqueous solution can provide the  
37 desired stoichiometric mixture at the molecular level. The resulting stable and homogeneous  
38 solution ensures precisely control of the stoichiometry and spatial uniformity for the films.  
39  
40  
41  
42  
43  
44  
45  
46  
47  
48  
49  
50  
51  
52  
53  
54  
55  
56  
57  
58  
59  
60

1  
2  
3 Adjustment of the stoichiometry results in different bandgaps for the CZTGSSe films ranging  
4 from 1.05 eV to 1.95 eV. In this work, as one typical example of CZTGSSe thin films, CZTSSe  
5 film prepared by the polymer-assisted aqueous method is demonstrated with a hall coefficient of  
6 +137 cm<sup>3</sup>/C and carrier mobility of 43 cm<sup>2</sup>/V·S at room temperature, respectively. Moreover, the  
7 CZTSSe thin film, when used as the active layer in an inorganic solar cell, yields a power  
8 conversion efficiency of 3.55 %.

## 17 RESULTS AND DISCUSSION

19 The schematic diagram of precursor preparation process and annealing process are shown in  
20 **Figure 1**. To investigate the thermal decomposition of the precursor thin film, we utilize  
21 TG/DTA 7300 to trace the thermal behaviors of the mixed metal precursor solution under an  
22 argon atmosphere. **Figure 2(a)** shows that the sample begins to decompose at 200 °C and stops  
23 at around 450 °C. This suggests that the polymer is almost completely decomposed and that  
24 CZTGSSe thin films may be obtained above 450 °C. The mass spectroscopy data from a typical  
25 decomposition process (**Figure S1**) shows that the polymer decomposes into a molecular gas  
26 during the thermal treatment. The small gaseous molecules are swept away by the gas flow  
27 leaving behind pure metal atoms, which results in the growth of high-quality thin films. It is  
28 worth noting that the crystallinity of the resultant thin films is influenced by the annealing  
29 process and temperature. X-ray diffraction patterns (XRD) (**Figure 2(b)** and **Figure 2(c)**) were  
30 used to identify the crystal structures of the CZTGSSe thin films. All the peaks in the XRD data  
31 from samples A, C, E can be assigned to kesterite CZTSe (JCPDS: 52-0868), CZTS (JCPDS: 26-  
32 0575) and CZGS (JCPDS: 78-781). The prominent peaks at ca. 28.5°, 33.0°, 47.3°, and 56.2° can  
33 be indexed to the (112) (200) (220), and (312) orientations for CZTGSSe. It is interesting to see  
34 that all the major peaks have regular shifts from samples A to E. **Figure 2(c)** shows the trend of  
35  
36  
37  
38  
39  
40  
41  
42  
43  
44  
45  
46  
47  
48  
49  
50  
51  
52  
53  
54  
55  
56  
57  
58  
59  
60

1  
2  
3 the peak corresponding to the (112) peak. The shifts can be attributed to changing atomic mass.  
4  
5 By replacing the lighter (smaller) S atom (1.84 Å) with heavier (larger) Se atom (1.98 Å) in a  
6  
7 CZTS lattice after the selenization process, the diffraction peak in XRD pattern of sample B  
8  
9 shows a distinct shift to lower (two-theta) angles compared with sample C due to the  
10  
11 corresponding expansion in the unit cell. The Se/(Se+S) ratio can be calculated to be 0.32 based  
12  
13 on the shift of the two-theta angles. A similar trend in XRD pattern for sample D is found when  
14  
15 some Sn atoms are substituted by Ge atoms. In this case the ratio Ge/(Ge+Sn) is 0.41. Apart  
16  
17 from the shifts, no unidentified peaks or peaks from secondary phases were observed in any of  
18  
19 the XRD spectra. Based on the above analyses, samples A, B, C, D and E in **Figure 2(b)**  
20  
21 correspond to the following thin films:  $\text{Cu}_2\text{ZnSnSe}_4$  (CZTSe),  $\text{Cu}_2\text{ZnSn}(\text{S}, \text{Se}_4)$  (CZTSSe),  
22  
23  $\text{Cu}_2\text{ZnSnS}_4$  (CZTS),  $\text{Cu}_2\text{Zn}(\text{Sn}, \text{Ge})\text{S}_4$  (CZTGS) and  $\text{Cu}_2\text{ZnGeS}_4$  (CZGS), respectively. As is well  
24  
25 known, XRD patterns are insufficient to confirm the phase purity of CZTGSSe structures due to  
26  
27 similar diffraction peaks of binary and ternary chalcogenides.<sup>19</sup> Here, Raman spectroscopy is  
28  
29 employed to confirm the purity of the thin films. For the Raman spectroscopy of such thin films  
30  
31 (**Figure 2(d)**), major characteristic peaks appear at  $286 \text{ cm}^{-1}$  and  $336 \text{ cm}^{-1}$  for sample C,  
32  
33 corresponding to CZTS as previously reported.<sup>20-23</sup> No evidence of other possible binary phases  
34  
35 ( $\text{Cu}_2\text{S}$ ,  $\text{ZnS}$ ,  $\text{Cu}_2\text{SnS}_3$ ) appear in the Raman spectra.<sup>24</sup> For sample A, the major peak shifts to  $194$   
36  
37  $\text{cm}^{-1}$  which is consistent with the reported value for CZTSe.<sup>25, 26</sup> It is found that the Raman  
38  
39 spectra show a systematic shift to a lower wavenumber as one substitutes the smaller S atoms  
40  
41 with larger Se atoms. On the other hand, the major peaks are shifted to larger wavenumber along  
42  
43 when replacing Sn atoms with Ge atoms. While the Sn atoms are completely substituted by Ge  
44  
45 for sample E, the two strong peaks at  $360 \text{ cm}^{-1}$  and  $291 \text{ cm}^{-1}$  can be assigned to CZGS thin  
46  
47  
48  
49  
50  
51  
52  
53  
54  
55  
56  
57  
58  
59  
60

1  
2  
3 films.<sup>27</sup> Thus, in combination, the XRD and Raman spectroscopic data confirm high purity of  
4  
5 CZTGSSe thin films are grown by our aqueous solution approach.  
6  
7

8  
9 The valence states of the constituent elements about CZTSSe and CZTGS are investigated  
10 by X-ray Photoelectron Spectroscopy (XPS). **Figure 3(a)** is the full spectrum of CZTSSe thin  
11 film, it indicates that the thin film contains Cu, Zn, Sn, S, Se, and C elements. **Figure 3(b-f)** are  
12 the high-resolution spectra of Cu 2p, Zn 2p, Sn 3d, S 2p, and Se 2p. As can be seen, the binding  
13 energy value of Cu 2p are 951.60 eV and 931.82 eV with a peak splitting of 19.78 eV, which is  
14 correspond to the Cu<sup>+</sup>. It can be illustrated that the Cu<sup>2+</sup> has been reduced to Cu<sup>+</sup> during the  
15 progress. The peaks show binding energy value of Zn 2p at 1044.62 eV and 1021.62 eV with a  
16 separation of 23.0 eV, which is consistent with divalent Zn<sup>2+</sup>. The spectrum of Sn 3d exhibits  
17 two characteristic peaks at 494.72 eV and 486.22 eV with a split orbit of 8.5 eV. It suggests that  
18 the Sn<sup>2+</sup> have been oxidized to Sn<sup>4+</sup> during the grown progress. This shows the Cu<sup>2+</sup> phase is  
19 reduced to Cu<sup>+</sup> while Sn<sup>2+</sup> is oxidized to Sn<sup>4+</sup> during the growth progress.<sup>8, 28</sup> Meanwhile, the  
20 spectra of S can be fitted to two peaks which are assigned to S 2p. The peaks at 55.3 and 54.6 eV  
21 are corresponding to the Se 2p. Therefore, these results are in line with the reported values of the  
22 binding energy of the elements forming CZTSSe, further confirming the phase purity of the  
23 synthesized CZTSSe. Furthermore, the XPS spectra (**Figure S2**) of CZTGS thin film were  
24 exhibited, which illustrated the pure CZTGS was grown.  
25  
26  
27  
28  
29  
30  
31  
32  
33  
34  
35  
36  
37  
38  
39  
40  
41  
42  
43  
44  
45

46 The surface morphology and layer properties of the deposited CZTSSe thin films were also  
47 investigated. **Figure 4(a, c)** and **4(b, d)** show the film has a dense and uniform structure, which  
48 is free of cracks. The average grain size is about 85 nm. Cross-sectional SEM studies show the  
49 thin film has a homogeneous thickness and a sharp interface between the film and the substrate.  
50 The thickness of the films is about 2 μm after spin-coating 5 times. It is worth noting that the  
51  
52  
53  
54  
55  
56  
57  
58  
59  
60

1  
2  
3 thickness of the film could be adjusted with different spin-coating repetition times. Elemental  
4 mapping (**Figure S3 (a-g)**) of the CZTSSe film is helpful to understand the elemental  
5 distribution. The different colors (**Figure S3 (a-g)**) of yellow, green, blue, red, pink, light blue  
6 and white represent Cu, Zn, Sn, S, Se, C and O, respectively. The uniform colors suggest that the  
7 five major elements (Cu, Zn, Sn, S, Se) are homogeneously distributed in the film. Upon  
8 combining all five elemental maps in **Figure S3 (h)**, the uniform colorful image further confirms  
9 the compositional purity of the film, which is consistent with the results obtained from XRD and  
10 Raman spectroscopy. It is noting that the EDX data in **Table S1** shows the CZTGSSe thin films  
11 have a copper-poor and zinc-rich conditions.<sup>29</sup> Some literatures report that the copper-poor and  
12 zinc-rich films tend to have better device performance applying to inorganic solar cells.<sup>30</sup>

13  
14  
15  
16  
17  
18  
19  
20  
21  
22  
23  
24  
25  
26  
27  
28  
29  
30  
31  
32  
33  
34  
35  
36  
37  
38  
39  
40  
41  
42  
43  
44  
45  
46  
47  
48  
49  
50  
51  
52  
53  
54  
55  
56  
57  
58  
59  
60

The bandgap of the CZTGSSe thin films can be tuned by varying an elemental component. Usually, there are four components (Sn, Ge, S, and Se) influencing the bandgap of CZTGSSe. The bandgap of CZTSSe can be tuned between 1.0 eV to 1.5 eV by adjusting the ratio of Se/(Se+S).<sup>8, 31, 32</sup> Similarly, the bandgap of CZTGS can be manipulated between 1.5 eV to 2.25 eV by adjusting of the Sn and Ge compositions.<sup>14, 33, 34</sup> The bandgap of the CZTGSSe thin films prepared in this work can be calculated through their UV-Vis absorption spectra (**Figure S4**). The relationship of the optical absorption coefficient ( $\alpha$ ) and optical bandgap ( $E_g$ ) of the thin films is given by the following formula (1):

$$(Ah\nu) = A(h\nu - E_g)^m \quad (1)$$

Where A is a constant and the exponent value ( $m$ ) is 1/2 for a direct band transition. Therefore, the  $E_g$  of  $\text{Cu}_2\text{Zn}(\text{Sn, Ge})(\text{S, Se})_4$  with direct band transitions can be calculated by formula (2):

$$(Ah\nu)^2 = A(h\nu - E_g) \quad (2)$$

The optical bandgap is obtained by extrapolating the linear part of the plot  $(ah\nu)^2$  versus  $h\nu$  (**Figure 5(a)**). The result indicates that the bandgap of CZTS thin films is 1.55 eV. As the S atoms are substituted by Se, the bandgap decreases to 1.05 eV. For Se/(Se+S) of 0.32, the bandgap of CZTSSe obtained from the plot  $(ah\nu)^2$  versus  $h\nu$  is 1.35 eV. Meanwhile, the bandgap of CZTSSe(Se/(Se+S)=x) can be modeled by Vegard's law using the following equation:

$$E_g(x) = (1-x)E_g(\text{CZTS}) + xE_g(\text{CZTSe}) - bx(1-x) \quad (3)$$

Where b is a constant relating to the nonlinear relationship between the bandgap and the ratio of Se/(Se+S). According to the calculation, the bandgap of CZTSSe, is about 1.37eV, which is in good agreement with the experimental value. Similarly, the bandgap of CZTGS films increases as the Ge content is increased (by replacing Sn atoms). For a ratio of Ge/(Ge+Sn) = 0.41, the bandgap of the CZTGS film extracted from the absorption plot is 1.67 eV, in close agreement to the theoretical value of 1.71 eV. When Ge completely replaces Sn, the bandgap of CZGS is estimated to be 1.95 eV. In short, the bandgap of CZTGSSe can be adjusted from 1.05 to 1.95 eV by controlling the Sn, Ge, S, and Se compositions.

The electrical properties of the thin films were evaluated by a physical properties measurement system (PPMS). An evaluation of the typical CZTSSe thin film was carried out using a four-probe van der Pauw method. As shown in **Figure 5(b)**, the film exhibits a resistivity of 3.17  $\Omega\text{cm}$  at room temperature. The resistivity gradually increases with decreasing temperature, suggesting semiconducting behavior. The Hall coefficient  $R_H$  is  $+137 \text{ cm}^3/\text{C}$  indicating the CZTSSe film to be *p*-type. The carrier concentration ( $n_s$ ) and Hall mobility ( $\mu$ ) can be calculated, according to the following equations (4) and (5),

$$n_s = \frac{1}{e} R_H \quad (4)$$

$$\mu = R_H / \rho \quad (5)$$

Where  $n_s$  is carrier concentration,  $e$  is the electron charge,  $R_H$  is Hall coefficient,  $\mu$  is Hall mobility, and  $\rho$  is resistivity. The carrier concentration and Hall mobility are measured to be  $4.5 \times 10^{16} \text{ cm}^{-3}$  and  $43 \text{ cm}^2 \text{ V}^{-1} \text{ s}^{-1}$  at room temperature, respectively. The carrier concentration is similar to the other reports by Liu et al. ( $3.9 \times 10^{16} \text{ cm}^{-3}$ ) and Scragg et al. ( $1.7 \times 10^{16} \text{ cm}^{-3}$ ),<sup>35,36</sup> but lower than Nakazawa et al. ( $10^{18}$ - $10^{19} \text{ cm}^{-3}$ ) found.<sup>37</sup> The mobility of holes is higher than most of the other works. Liu et al. reported the mobility of CZTS film is  $30 \text{ cm}^2 \text{ V}^{-1} \text{ s}^{-1}$  and Tanaka et al. reported the hall mobility is about  $6.0 \text{ cm}^2 \text{ V}^{-1} \text{ s}^{-1}$ .<sup>35,38</sup> This suggests that our grown p-type CZTSSe films are of high quality and promising for optoelectronics applications.

With a suitable bandgap and good mobility of hole, the p-type CZTSSe thin film as an absorptive layer was assessed for its suitability in a solar cell. A typical solar cell was been fabricated with SLG/Mo/CZTSSe/CdS/ZnO/ITO/Ag layers. The physical image of the solar cell is shown in **Figure S5**. The device (**Figure 6(a)**) displays a  $J_{sc}$  of  $28.75 \text{ mA/cm}^2$ ,  $V_{oc}$  of  $0.39 \text{ V}$  and FF of  $0.317$ , yielding a conversion efficiency  $\sim 3.55 \%$ . Though the conversion efficiency is mediocre, it is comparable to solar cells that employ organic solvents.<sup>39, 40</sup> Such as H. W. Hillhouse group reported  $4.1 \%$  conversion efficiency with dimethyl sulfoxide solvent and Y. Yang et al. reported  $1.2\%$  by single-component precursor with hydrazine.<sup>41, 42</sup> **Figure 6(b)** shows EQE spectrum of the solar cell and exhibits a broad absorption from  $350$  to  $980 \text{ nm}$ . Without any optimization of the device, a high EQE over  $60\%$  ( $\sim 660 \text{ nm}$ ) has been achieved. The bandgap of the CZTSSe film in a solar cell was calculated to be  $1.35 \text{ eV}$  (inset of **Figure 6(b)**) which is in good agreement with the value estimated from the absorption spectrum. To analyze the device structure, the cross-section image of the device was investigated by SEM (**Figure 6(c)**). The

1  
2  
3 device includes Mo substrate, CZTSSe layer, and CdS/ZnO/In-doped SnO<sub>2</sub>(ITO)layer.  
4  
5 Surprising to find that CZTSSe layer consists a small grain layer about 1200 nm and a large layer  
6  
7 about 300 nm. The cross-section morphology of the CZTSSe layer is different from that grown  
8  
9 on a quartz substrate. The different morphology is resulting from the annealing process. The  
10  
11 CZTSSe grown on quartz is annealed from the room-temperature at a rate of 5 °C/min to 520°C  
12  
13 and maintained at 520°C for 20 min, while the CZTSSe active layer in the solar cell is annealed  
14  
15 by a rapid thermal process (RTP). It indicates that the large grain CZTSSe layer is grown during  
16  
17 the RTP. The interface between the small grain layer and the large grain layer may be not an  
18  
19 ideal structure, and the small grain CZTSSe layer will hindrance the electrons' and holes'  
20  
21 transportation.<sup>43</sup> Thereby the small grain CZTSSe layer will affect the performance of the device.  
22  
23  
24  
25  
26 To analyze the element distribution in the device, the SEM-EDAX-Line (**Figure 6 (d)**) is  
27  
28 measured at the cross-section of the device according to the arrows direction as **Figure 6 (c)**  
29  
30 shown. The Cu, Zn, Sn atoms show a uniform distribution in the active layer. However, the Se  
31  
32 atom percent show a higher ratio in the large grain layer than the small grain layer and there is a  
33  
34 carbon content in the small grain CZTSSe layer from the carbon spectrum. Therefore a carbon  
35  
36 residue is impeding the formation of the large CZTSSe particles, resulting a high series  
37  
38 resistance and restricting the transport of photo-generated carriers and forming recombination,  
39  
40 thereby deteriorate to the performance of the device. A lot of methods have been proposed to  
41  
42 improve the quality of the CZTSSe activity layer, the small grain layer is still existence yet. So  
43  
44 the continued optimization of the CZTSSe activity layer is a significant challenge in the future.  
45  
46  
47  
48  
49

## 50 51 CONCLUSIONS

52  
53 In summary, we report an environmental-friendly aqueous solution-based polymer assisted  
54  
55 deposition approach to growing high-quality Cu<sub>2</sub>Zn(Sn, Ge)(S, Se)<sub>4</sub> (CZTGSSe) thin films. The  
56  
57  
58  
59  
60

1  
2  
3 experimental results demonstrated CZTGSSe films can be easily tailored to fabricate with  
4 accurately controlled elemental compositions. Furthermore, the corresponding bandgaps of  
5 CZTGSSe thin films are readily tuned from 1.05 eV to 1.95 eV by changing the Sn, Ge, S, and  
6 Se composition in the aqueous precursor solution. A representative CZTSSe film exhibits good  
7 electrical properties along with optical properties and high charge mobility. Carrier transport  
8 measurements also indicated that a hall coefficient of  $+137 \text{ cm}^3/\text{C s}$  was achieved on one of our  
9 as-grown  $\text{Cu}_2\text{Zn}(\text{Sn, Ge})(\text{S, Se})_4$  thin films. Meanwhile, other performance metrics including the  
10 resistivity, concentration and carrier mobility of the  $\text{Cu}_2\text{ZnSn}(\text{S,Se})_4$  thin film are meeting  
11 practical applications with values of  $3.17 \text{ ohm}\cdot\text{cm}$ ,  $4.5 \times 10^{16} \text{ cm}^{-3}$  and  $43 \text{ cm}^2/\text{V}\cdot\text{S}$  at room  
12 temperature, respectively. Importantly, the  $\text{Cu}_2\text{ZnSn}(\text{S,Se})_4$  thin film, used as an active layer in a  
13 solar cell, yields a power conversion efficiency of 3.55%. Therefore, the feasible growth of  
14  $\text{Cu}_2\text{Zn}(\text{Sn, Ge})(\text{S, Se})_4$  thin films *via* an environmental benign aqueous system provides an  
15 effective pathway to fabricate a variety of single/multi metal films for solar energy applications  
16 and other solution-processed optoelectronic devices.  
17  
18  
19  
20  
21  
22  
23  
24  
25  
26  
27  
28  
29  
30  
31  
32  
33  
34  
35

### 36 ACKNOWLEDGMENTS

37  
38  
39 We gratefully acknowledge the support from "973 Program---the National Basic Research  
40 Program of China" Special Funds for the Chief Young Scientist (2015CB358600), the Excellent  
41 Young Scholar Fund from National Natural Science Foundation of China (21422103), Jiangsu  
42 Young Scholar Fund from National Natural Science Foundation of China (21422103), Jiangsu  
43 Fund for Distinguished Young Scientist (BK20140010), the Priority Academic Program  
44 Development of Jiangsu Higher Education Institutions (PAPD), and Jiangsu Scientific and  
45 Technological Innovation Team (2013).  
46  
47  
48  
49  
50  
51  
52  
53

54 **Supporting Information.** The detailed experimental section, the decomposed progress of a  
55 typical precursor solution; the mass spectrum of the decomposed products; XPS analysis,  
56  
57  
58  
59  
60

UV-Vis spectra, element ratio table of CZTGSSe thin films and the structure of the solar cell are included in the supporting information.

## AUTHOR INFORMATION

### Corresponding Author

\* Email: [zouguifu@suda.edu.cn](mailto:zouguifu@suda.edu.cn)

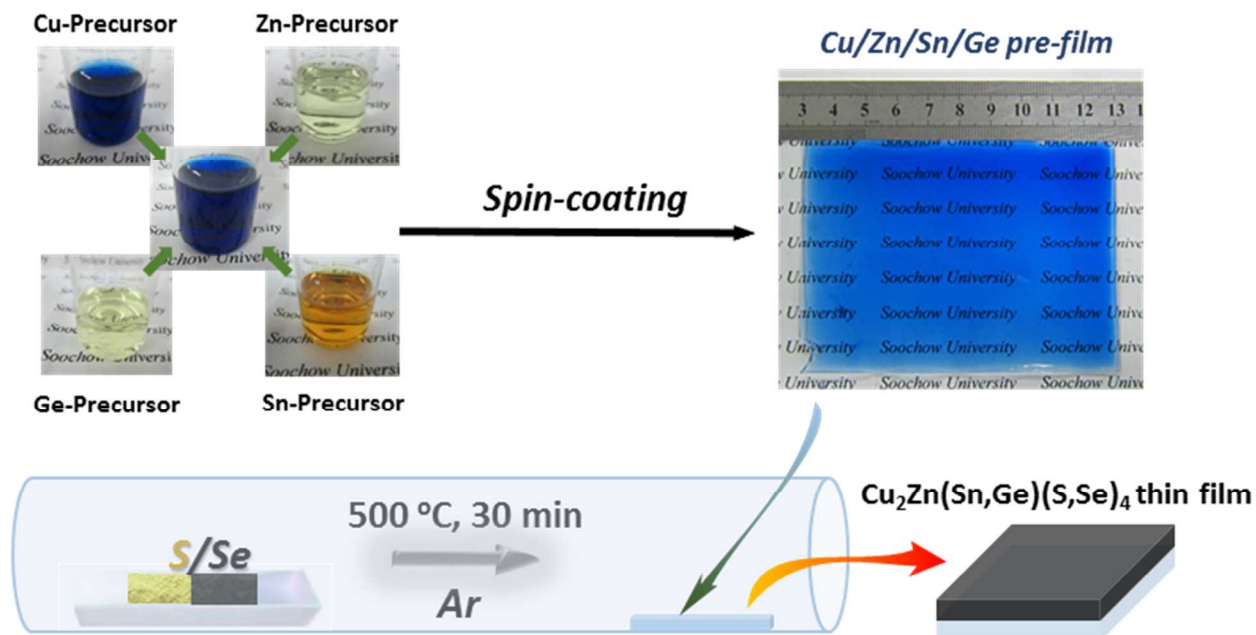
### Author Contributions

The manuscript was written through contributions of all authors. All authors have given approval to the final version of the manuscript.

### Notes

The authors declare no competing financial interest.

## FIGURES



1  
2  
3  
4  
5  
6  
7  
8  
9  
10  
11  
12  
13  
14  
15  
16  
17  
18  
19  
20  
21  
22  
23  
24  
25  
26  
27  
28  
29  
30  
31  
32  
33  
34  
35  
36  
37  
38  
39  
40  
41  
42  
43  
44  
45  
46  
47  
48  
49  
50  
51  
52  
53  
54  
55  
56  
57  
58  
59  
60

**Figure 1.** schematic illustration of precursor preparation progress and thin film annealing progress.

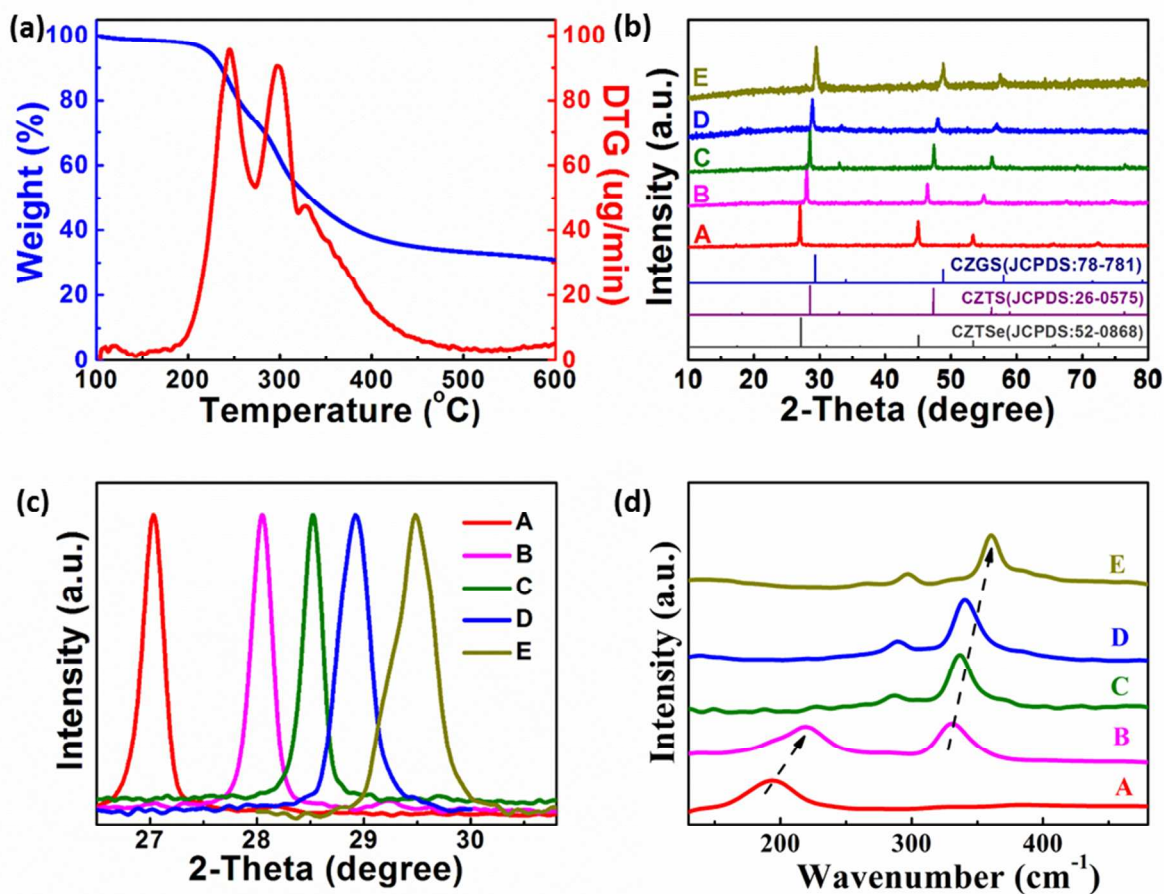


**Figure 2.** (a) Thermal gravimetric analysis (TGA) curve of CuZn(Sn,Ge) precursor solution. (b) XRD patterns of CZTGSSe thin films. (c) The normalized (112) diffraction peak of all samples. (d) Raman spectra of CZTGSSe thin films (A: CZTSe, B: CZTSSe, C: CZTS, D: CZTGS, E: CZGS).

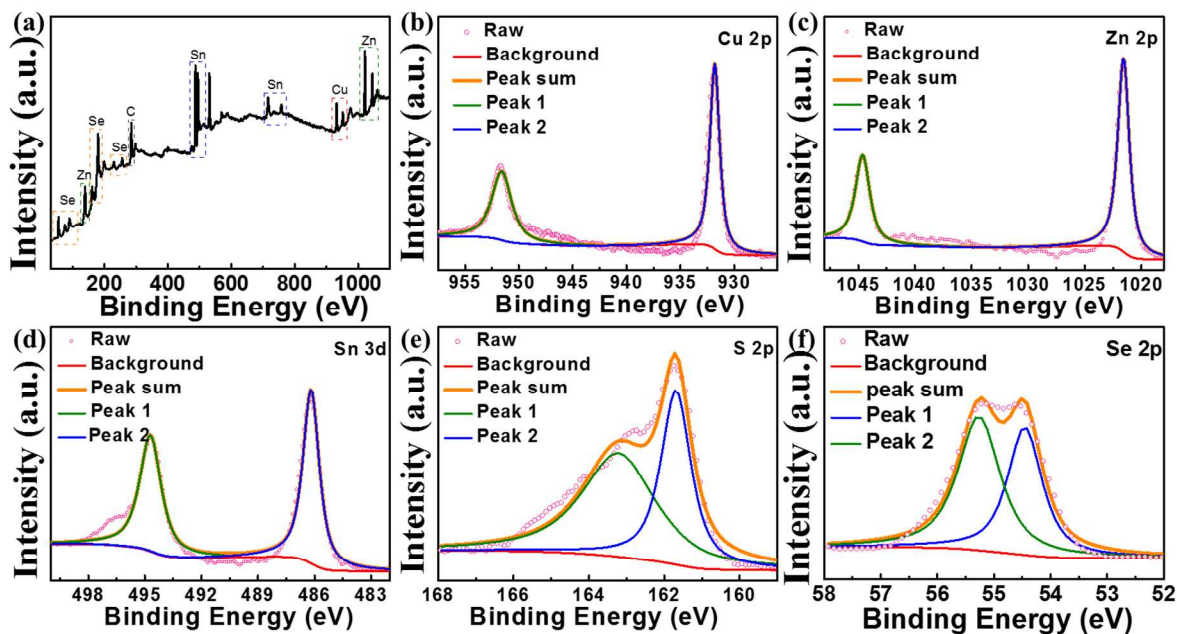


**Figure 3.** The XPS analysis of the CZTSSe thin films (a) full spectra, (b)Cu 2p core level, (c)Zn 2p core level,(d) Sn 3d core level, (e) S 2p core level and (f) Se 2p core level.

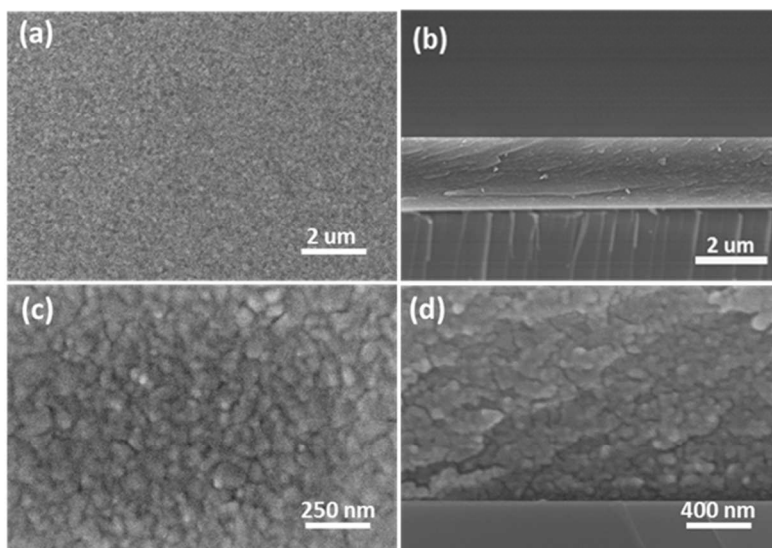


**Figure 4.** (a, c) Top-view and (b, d) Cross-section images of CZTSSe thin films.

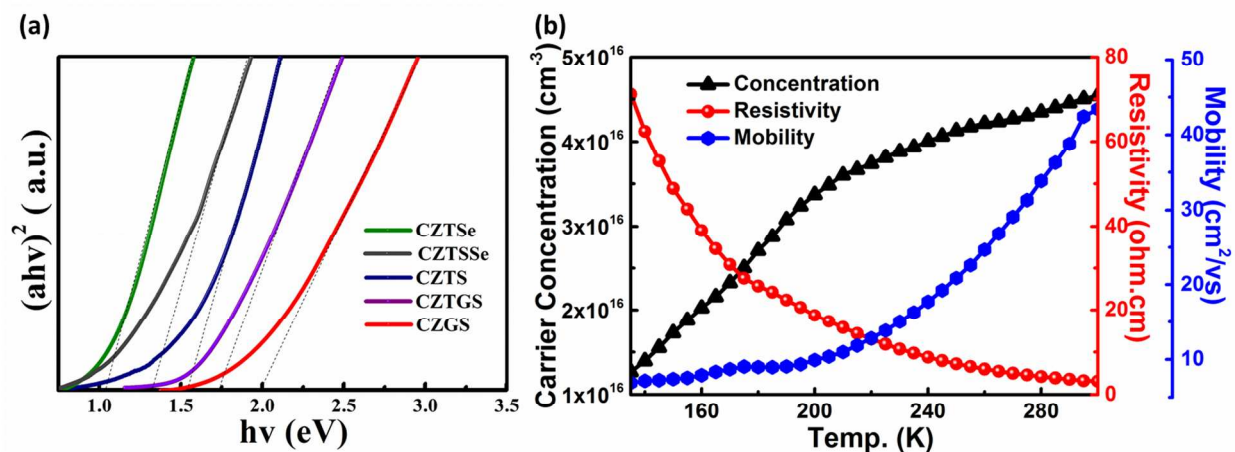


**Figure 5.** (a) The band gap values of obtained  $\text{Cu}_2\text{Zn}(\text{Sn}, \text{Ge})(\text{S}, \text{Se})_4$  thin films, evaluated from the plots of  $(ah\nu)^2$  vs.  $h\nu$ . (b) The temperature dependence of resistivity, concentration and mobility of the CZTSSe thin films, respectively.

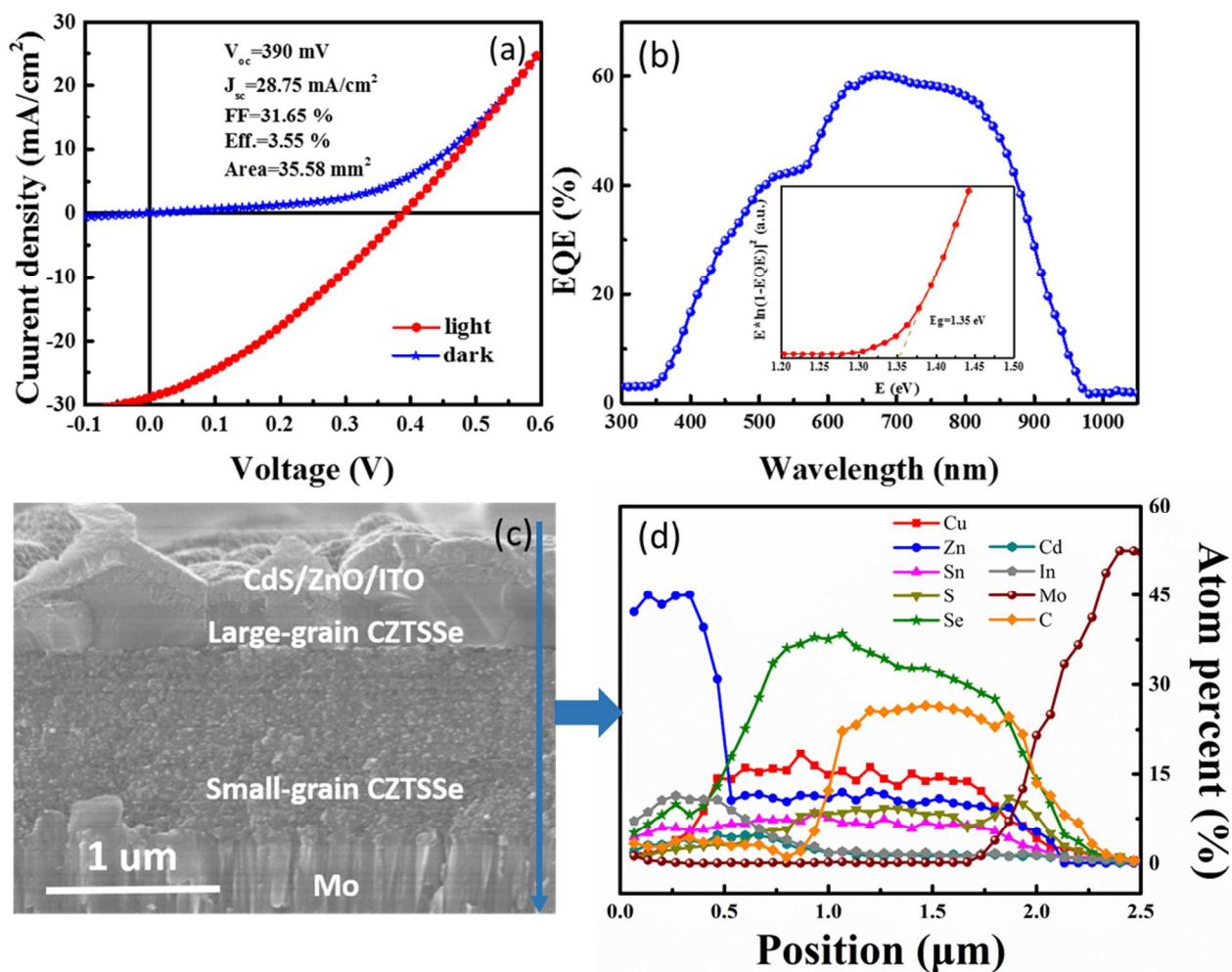


**Figure 6.** (a) The current density-voltage ( $J$ - $V$ ) characteristics, (b) EQE plot of the CZTSSe solar cell, respectively. Inset, the bandgap is calculated by  $[E \cdot \ln(1 - \text{EQE})]^2$  vs.  $E$  curve. Cell area:  $0.3558 \text{ cm}^2$ , (c) the cross-section SEM image of a CZTSSe solar cell, (d) the compositional distributions of CZTSSe solar cell was tested via SEM-EDAX-line scan.

## REFERENCES

- (1) Yu, X.; Shavel, A.; An, X.; Luo, Z.; Ibanez, M.; Cabot, A.  $\text{Cu}_2\text{ZnSnS}_4$ -Pt and  $\text{Cu}_2\text{ZnSnS}_4$ -Au Heterostructured Nanoparticles for Photocatalytic Water Splitting and Pollutant Degradation. *J. Am. Chem. Soc.* **2014**, *136*, 9236-9239.
- (2) Xin, X.; He, M.; Han, W.; Jung, J.; Lin, Z. Low-cost Copper Zinc Tin Sulfide Counter Electrodes for High-efficiency Dye-sensitized solar cells. *Angew. Chem. Int. Ed.* **2011**, *50*, 11739-11742.
- (3) Todorov, T. K.; Tang, J.; Bag, S.; Gunawan, O.; Gokmen, T.; Zhu, Y.; Mitzi, D. B. Beyond 11 % Efficiency: Characteristics of State-of-the-Art  $\text{Cu}_2\text{ZnSn}(\text{S},\text{Se})_4$  Solar Cells. *Adv. Energy Mater.* **2013**, *3*, 34-38.
- (4) Mitzi, D. B.; Yuan, M.; Liu, W.; Kellock, A. J.; Chey, S. J.; Deline, V.; Schrott, A. G. A High-Efficiency Solution-Deposited Thin-Film Photovoltaic Device. *Adv. Mater.* **2008**, *20*, 3657-3662.
- (5) Yang, W.; Duan, H. S.; Bob, B.; Zhou, H.; Lei, B.; Chung, C. H.; Li, S. H.; Hou, W. W.; Yang, Y. Novel Solution Processing of High-efficiency Earth-abundant  $\text{Cu}_2\text{ZnSn}(\text{S},\text{Se})_4$  solar cells. *Adv. Mater.* **2012**, *24*, 6323-6329.
- (6) Siebentritt, S.; Schorr, S. Kesterites-A Challenging Material for Solar Cells. *Prog. Photovolt: Res. Appl.* **2012**, *20*, 512-519.
- (7) Panthani, M. G.; Khan, T. A.; Reid, D. K.; Hellebusch, D. J.; Rasch, M. R.; Maynard, J. A.; Korgel, B. A. In Vivo Whole Animal Fluorescence Imaging of

1  
2  
3 A Microparticle-based Oral Vaccine Containing (CuInSe<sub>x</sub>S<sub>2-x</sub>)/ZnS Core/Shell  
4 Quantum Dots. *Nano Lett.* **2013**, *13*, 4294-4298.  
5  
6

7  
8  
9 (8) Ji, S.; Shi, T.; Qiu, X.; Zhang, J.; Xu, G.; Chen, C.; Jiang, Z.; Ye, C. A Route to  
10 Phase Controllable Cu<sub>2</sub>ZnSn(S<sub>1-x</sub>Se<sub>x</sub>)<sub>4</sub> Nanocrystals with Tunable Energy  
11 Bands. *Sci. Rep.* **2013**, *3*, 2733.  
12  
13  
14

15  
16  
17 (9) Bag, S.; Gunawan, O.; Gokmen, T.; Zhu, Y.; Mitzi, D. B. Hydrazine-Processed  
18 Ge-Substituted CZTSe Solar Cells. *Chem. Mater.* **2012**, *24*, 4588-4593.  
19  
20  
21

22  
23 (10) Yang, W.; Duan, H. S.; Cha, K. C.; Hsu, C. J.; Hsu, W. C.; Zhou, H.; Bob, B.;  
24 Yang, Y. Molecular Solution Approach to Synthesize Electronic Quality  
25 Cu<sub>2</sub>ZnSnS<sub>4</sub> Thin Films. *J. Am. Chem. Soc.* **2013**, *135*, 6915-6920.  
26  
27  
28

29  
30  
31 (11) Kim, I.; Kim, K.; Oh, Y.; Woo, K.; Cao, G.; Jeong, S.; Moon, J. Bandgap-  
32 Graded Cu<sub>2</sub>Zn(Sn<sub>1-x</sub>Ge<sub>x</sub>)S<sub>4</sub> Thin-Film Solar Cells Derived from Metal  
33 Chalcogenide Complex Ligand Capped Nanocrystals. *Chem. Mater.* **2014**, *26*,  
34 3957-3965.  
35  
36  
37  
38

39  
40  
41 (12) Wang, W.; Winkler, M. T.; Gunawan, O.; Gokmen, T.; Todorov, T. K.; Zhu,  
42 Y.; Mitzi, D. B. Device Characteristics of CZTSSe Thin-Film Solar Cells with  
43 12.6 % Efficiency. *Adv. Energy Mater.* **2014**, *4*, 1301465.  
44  
45  
46  
47

48  
49  
50 (13) Ibanez, M.; Zamani, R.; LaLonde, A.; Cadavid, D.; Li, W.; Shavel, A.; Arbiol,  
51 J.; Morante, J. R.; Gorsse, S.; Snyder, G. J.; Cabot, A. Cu<sub>2</sub>ZnGeSe<sub>4</sub>  
52 Nanocrystals: Synthesis and Thermoelectric Properties. *J. Am. Chem. Soc.*  
53 **2012**, *134*, 4060-4063.  
54  
55  
56  
57  
58  
59  
60

- 1  
2  
3  
4 (14) Ford, G. M.; Guo, Q.; Agrawal, R.; Hillhouse, H. W. Earth Abundant Element  
5  
6  $\text{Cu}_2\text{Zn}(\text{Sn}_{1-x}\text{Ge}_x)\text{S}_4$  Nanocrystals for Tunable Band Gap Solar Cells: 6.8 %  
7  
8 Efficient Device Fabrication. *Chem. Mater.* **2011**, *23*, 2626-2629.  
9  
10  
11 (15) Tian, Q.; Huang, L.; Zhao, W.; Yang, Y.; Wang, G.; Pan, D. Metal Sulfide  
12  
13 Precursor Aqueous Solutions for Fabrication of  $\text{Cu}_2\text{ZnSn}(\text{S},\text{Se})_4$  Thin Film  
14  
15 Solar Cells. *Green Chem.* **2015**, *17*, 1269-1275.  
16  
17  
18  
19 (16) S. Y. Wei, Y. C. Liao, C. H. Hsu, C. H. Cai, W. C. Huang, M. C. Huang, C. H.  
20  
21 Lai, *Nano Energy* 26(2016,)74-82.  
22  
23  
24  
25 (17) Jia, Q. X.; McCleskey, T. M.; Burrell, A. K.; Lin, Y.; Collis, G. E.; Wang, H.;  
26  
27 Li, A. D.; Foltyn, S. R. Polymer-assisted Deposition of Metal-oxide Films. *Nat.*  
28  
29 *Mater.* **2004**, *3*, 529-532.  
30  
31  
32  
33 (18) Zou, G. F.; Zhao, J.; Luo, H. M.; McCleskey, T. M.; Burrell, A. K.; Jia, Q. X.  
34  
35 Polymer-assisted-deposition: A Chemical Solution Route for A Wide Range of  
36  
37 Materials. *Chem. Soc. Rev.* **2013**, *42*, 439-449.  
38  
39  
40  
41 (19) Scragg, J. J.; Ericson, T.; Fontané, X.; Izquierdo-Roca, V.; Pérez-Rodríguez,  
42  
43 A.; Kubart, T.; Edoff, M.; Platzer-Björkman, C. Rapid Annealing of Reactively  
44  
45 Sputtered Precursors for  $\text{Cu}_2\text{ZnSnS}_4$  Solar Cells. *Prog. Photovolt: Res. Appl.*  
46  
47 **2014**, *22*, 10-17.  
48  
49  
50  
51 (20) Sun, Y.; Zhang, Y.; Wang, H.; Xie, M.; Zong, K.; Zheng, H.; Shu, Y.; Liu, J.;  
52  
53 Yan, H.; Zhu, M.; Lau, W. Novel Non-hydrazine Solution Processing of Earth-  
54  
55  
56  
57  
58  
59  
60

1  
2  
3 Abundant  $\text{Cu}_2\text{ZnSn}(\text{S}, \text{Se})_4$  Absorbers for Thin-film Solar Cells. *J. Mater.*  
4  
5 *Chem. A* **2013**, *1*, 6880-6887.  
6  
7

8  
9 (21) Yang, W. C.; Miskin, C. K.; Carter, N. J.; Agrawal, R.; Stach, E. A.  
10  
11 Compositional Inhomogeneity of Multinary Semiconductor Nanoparticles: A  
12  
13 Case Study of  $\text{Cu}_2\text{ZnSnS}_4$ . *Chem. Mater.* **2014**, *26*, 6955-6962.  
14  
15

16  
17 (22) Wang, G.; Zhao, W.; Cui, Y.; Tian, Q.; Gao, S.; Huang, L.; Pan, D. Fabrication  
18  
19 of A  $\text{Cu}_2\text{ZnSn}(\text{S}, \text{Se})_4$  Photovoltaic Device by A Low-toxicity Ethanol Solution  
20  
21 Process. *ACS Appl. Mater. Interfaces* **2013**, *5*, 10042-10047.  
22  
23

24  
25 (23) Tan, J. M.; Lee, Y. H.; Pedireddy, S.; Baikie, T.; Ling, X. Y.; Wong, L. H.  
26  
27 Understanding The Synthetic Pathway of A Single-phase Quarternary  
28  
29 Semiconductor Using Surface-enhanced Raman Scattering: A Case of Wurtzite  
30  
31  $\text{Cu}_2\text{ZnSnS}_4$  nanoparticles. *J. Am. Chem. Soc.* **2014**, *136* 18, 6684-6692.  
32  
33  
34

35  
36 (24) Altamura, G.; Vidal, J. Impact of Minor Phases on the Performances of  
37  
38 CZTSSe Thin Film Solar Cells. *Chem. Mater.* **2016**, *28*, 3540-3563.  
39  
40

41  
42 (25) Martin, T. R.; Katahara, J. K.; Bucherl, C. N.; Krueger, B. W.; Hillhouse, H.  
43  
44 W.; Luscombe, C. K. Nanoparticle Ligands and Pyrolyzed Graphitic Carbon in  
45  
46 CZTSSe Photovoltaic Devices. *Chem. Mater.* **2016**, *28*, 135-145.  
47  
48

49  
50 (26) Kumar, M.; Dubey, A.; Adhikari, N.; Venkatesan, S.; Qiao, Q. Strategic  
51  
52 Review of Secondary Phases, Defects and Defect-complexes in Kesterite  
53  
54 CZTSSe Solar Cells. *Energy Environ. Sci.* **2015**, *8*, 3134-3159.  
55  
56  
57  
58  
59  
60

- 1  
2  
3 (27) Khadka, D. B.; Kim, J. Study of Structural and Optical Properties of Kesterite  
4  
5  $\text{Cu}_2\text{ZnGeX}_4$  (X = S, Se) Thin Films Synthesized by Chemical Spray Pyrolysis.  
6  
7  
8 *Cryst. Eng. Comm.* 2013, 15, 10500.  
9
- 10  
11 (28) Singh, A.; Coughlan, C.; Milliron, D. J.; Ryan, K. M. Solution Synthesis and  
12  
13 Assembly of Wurtzite-Derived Cu–In–Zn–S Nanorods with Tunable  
14  
15 Composition and Band Gap. *Chem. Mater.* 2015, 27, 1517-1523.  
16  
17  
18
- 19 (29) Ahmed, S.; Reuter, K. B.; Gunawan, O.; Guo, L.; Romankiw, L. T.; Deligianni,  
20  
21 H. A High Efficiency Electrodeposited  $\text{Cu}_2\text{ZnSnS}_4$  Solar Cell. *Adv. Energy*  
22  
23 *Mater.* 2012, 2, 253-259.  
24  
25  
26
- 27 (30) Cao, Y.; Denny, M. S., Jr.; Caspar, J. V.; Farneth, W. E.; Guo, Q.; Ionkin, A.  
28  
29 S.; Johnson, L. K.; Lu, M.; Malajovich, I.; Radu, D.; Rosenfeld, H. D.;  
30  
31 Choudhury, K. R.; Wu, W. High-Efficiency Solution-Processed  
32  
33  $\text{Cu}_2\text{ZnSn}(\text{S},\text{Se})_4$  Thin-film Solar Cells Prepared from Binary and Ternary  
34  
35 Nanoparticles. *J. Am. Chem. Soc.* 2012, 134, 15644-15647.  
36  
37  
38
- 39 (31) Singh, A.; Singh, S.; Levchenko, S.; Unold, T.; Laffir, F.; Ryan, K. M.  
40  
41 Compositionally Tunable Photoluminescence Emission in  $\text{Cu}_2\text{ZnSn}(\text{S}_{1-x}\text{Se}_x)_4$   
42  
43 Nanocrystals. *Angew. Chem. Int. Ed.* 2013, 52, 9120-9124.  
44  
45  
46
- 47 (32) Fan, F. J.; Wu, L.; Gong, M.; Liu, G.; Wang, Y. X.; Yu, S. H.; Chen, S.; Wang,  
48  
49 L. W.; Gong, X. G. Composition and Band-gap-tunable Synthesis of Wurtzite-  
50  
51 derived  $\text{Cu}_2\text{ZnSn}(\text{S}_{1-x}\text{Se}_x)_4$  Nanocrystals: Theoretical and Experimental  
52  
53 Insights. *ACS Nano* 2013, 7, 1454-1463.  
54  
55  
56  
57  
58  
59  
60

- 1  
2  
3  
4  
5  
6  
7  
8  
9  
10  
11  
12  
13  
14  
15  
16  
17  
18  
19  
20  
21  
22  
23  
24  
25  
26  
27  
28  
29  
30  
31  
32  
33  
34  
35  
36  
37  
38  
39  
40  
41  
42  
43  
44  
45  
46  
47  
48  
49  
50  
51  
52  
53  
54  
55  
56  
57  
58  
59  
60
- (33) Zong, K.; Lu, S.; Wang, H.; Sun, Y.; Zheng, H.; Liu, J.; Yan, H. Retracted Article: The Synthesis of  $\text{Cu}_2\text{Zn}(\text{Ge}_x\text{Sn}_{1-x})\text{Se}_4$  Nanocrystals with Tunable Band Gaps. *Cryst. Eng. Comm.* **2013**, *15*, 6942.
- (34) Zhao, W. G.; Pan, D. C.; Liu, S. F. Kesterite  $\text{Cu}_2\text{Zn}(\text{Sn,Ge})(\text{S,Se})_4$  Thin Film with Controlled Ge-doping for Photovoltaic Application. *Nanoscale* **2016**, *8*, 10160-10165.
- (35) Liu, F.; Li, Y.; Zhang, K.; Wang, B.; Yan, C.; Lai, Y.; Zhang, Z.; Li, J.; Liu, Y. In Situ Growth of  $\text{Cu}_2\text{ZnSnS}_4$  Thin Films by Reactive Magnetron Co-sputtering. *Sol. Energy Mater. Sol. Cells* **2010**, *94*, 2431-2434.
- (36) Scragg, J. J.; Dale, P. J.; Peter L. M. Towards Sustainable Materials for Solar Energy Conversion: Preparation and Photoelectrochemical Characterization of  $\text{Cu}_2\text{ZnSnS}_4$ . *Electrochem. Commun.* **2008**, *10*, 639-642.
- (37) Nakayama, N.; Ito K. Sprayed Films of Stannite  $\text{Cu}_2\text{ZnSnS}_4$ . *Appl. Surface Sci.* **1996**, *92*, 171-175.
- (38) Tanaka, T.; Nagatomo, T.; Kawasaki, D.; Nishio, M.; Guo, Q.; Wakahara, A.; Yoshida, A.; Ogawa, H. Preparation of  $\text{Cu}_2\text{ZnSnS}_4$  Thin Films by Hybrid Sputtering. *J. Phys. Chem. Solids* **2005**, *66*, 1978-1981.
- (39) Guo, Q.; Hillhouse, H. W.; Agrawal, R. Synthesis of  $\text{Cu}_2\text{ZnSnS}_4$  Nanocrystal Ink and Its Use for Solar Cells. *J. Am. Chem. Soc.* **2009**, *131*, 11672-11673.

- 1  
2  
3 (40) Carrete, A.; Shavel, A.; Fontane, X.; Montserrat, J.; Fan, J.; Ibanez, M.;  
4  
5 Saucedo, E.; Perez-Rodriguez, A.; Cabot, A. Antimony-based Ligand  
6 Exchange to Promote Crystallization in Spray-Deposited  $\text{Cu}_2\text{ZnSnSe}_4$  Solar  
7 Cells. *J. Am. Chem. Soc.* **2013**, *135*, 15982-15985.  
8  
9  
10  
11  
12  
13  
14 (41) Zhou, H. P.; Duan, H. S.; Yang W. B.; Chen, Q.; Hsu, C. J.; Hsu, W. C.; Chen,  
15  
16 C. C.; Yang, Y. Facial Single-component Precursor for  $\text{Cu}_2\text{ZnSnS}_4$  with  
17 Enhanced Phase and Composition Controllability. *Energy Environ. Sci.* **2014**,  
18  
19  
20  
21  
22  
23  
24 (42) Ki, W.; Hillhouse, H. W. Earth-abundant Element Photovoltaics Directly from  
25  
26 Soluble Precursors with High Yield Using a Non-toxic Solvent. *Adv. Energy*  
27  
28  
29  
30  
31  
32  
33 (43) Embden, J. V.; Chesman, A. S. R.; Gaspera, E. D.; Duffy, N. W.; Watkins, S.  
34  
35 E.; Jasieniakov, J. J.  $\text{CuZnSnS}_{4x}\text{Se}_{4(1-x)}$  solar cells from polar nanocrystal inks.  
36  
37  
38  
39  
40  
41  
42  
43  
44  
45  
46  
47  
48  
49  
50  
51  
52  
53  
54  
55  
56  
57  
58  
59  
60

## TOC GRAPHIC

